Permanent emergency LED lamp based on a series single-switch resonant converter with battery clamp

Pablo Quintana-Barcia, *Member, IEEE*, Javier Ribas, *Senior Member, IEEE*, Francisco A. Juarez-Leon, *Member, IEEE*, and Diego Rodriguez-Fuertes

***Abstract*—Permanent emergency lighting is a safety device whose lamp is always on and continues to operate when a mains failure occurs. The circuit has to charge the battery and drive the lamp while the grid is present and keep the lamp running from the battery in case of mains failure. This might require up to three different converters: front-end converter, electronic ballast, and battery charger. Since an emergency lamp must be on for as long as the local regulations require during a grid failure, efficiency is key. This paper presents a permanent emergency lamp based on a series resonant current regulator that operates both as a ballast and as a battery charger. In this circuit, the power converter is placed in series with the LED array, operating as a controllable non-dissipative impedance. A methodology based on the study of energy balances during resonant operation intervals is presented, aiming to design and build a laboratory prototype with low component count and high efficiency.**

***Index Terms*—LED driver, permanent emergency lamp, resonant converter, single-switch topology.**

I. Introduction

EMERGENCY lighting is an effective life safety tool, developed to provide sufficient illumination when it is needed to escape quickly and safely from a building. Since emergency lighting is an indispensable safety system in buildings, its implementation, maintenance, and management is required by law. A number of standards have appeared for emergency lighting, defining the particular requirements for emergency permanent and non-permanent lighting systems, adequate location, installation, and testing of product to be considered [1]–[4]. Compliance to these specific standards is mandatory for all parties involved in the provision of emergency lighting: from the design/manufacturing company to the installer.

Emergency lighting units based on compact fluorescent lamps can be yet found in some buildings although the market tended to phase them out [5]. Despite these lamps can last up to 25,000 hours, low power (< 14 W) compact fluorescent lamps present a noticeable lower life time (< 5000 hours). This implies short lamp-replacement times and high maintenance costs. Nowadays, LED emergency fixtures are the predominant solution due to the well-known advantages of the LEDs: long lifespan (more than 50,000 hours), low power consumption and high efficacy. LEDs with luminous efficacies above 180 lm/W are currently available in the market, giving rise to the development of very compact lamps with optimal illumination levels. Moreover, the dimming capability of the LED makes this device very flexible. Therefore, less maintenance, smaller batteries, and better reliability is a common characteristic of LED emergency lamps.

There are different emergency lights available in the market: some of them keep a certain illumination level and increase/decrease it in case of a power cut while others stay turned off until the absence of the grid. Modern lamps may also include communications via DALI protocol [6]. However, no matter what, these lamps must comply with the aforementioned regulations in terms of type of batteries to be within, battery life, operation time during a power outage, charging rate, or illumination levels among others.

Depending on the nature of the emergency fixture (permanent or non-permanent), different solutions can be found. There is a wider variety in the market than in the literature. On one hand, if the lamp is non-permanent then a typical solution is to have an offline converter operating as a Power Factor Corrector (PFC)/battery charger, and a DC/DC converter to supply the lamp (see Fig. 1a) [7], [8]. In addition, a grid fault detector is also needed to turn on and off the LED driver. However, for low power applications, much cheaper solutions can be found in the market (e.g., charging the battery directly from the grid through a set of capacitors or even a transformer [9]).

On the other hand, if the lamp is permanent, then the LEDs are always in operation, supplied either by the grid or the battery. The cost reduction of LED technology has encouraged many local administrations in Europe to require the installation of permanent emergency lighting in a growing number of applications. Several solutions can be found in the literature:

1) Those involving three power converters: a battery charger, an LED driver and the front-end PFC. The main drawback of this solution is that three magnetic cores are required

Manuscript received June, 2021; revised July, 2021; accepted October, 2021. This work was supported in part by Ministry of Science and Innovation of the Government of Spain under Research Grant PID2019-105568RB-I00.

Pablo Quintana-Barcia, Javier Ribas and Diego Rodriguez-Fuertes are with the Efficient Energy Conversion, Industrial Electronics and Lighting Group (CE3I2), University of Oviedo, Gijon, Spain (contact author e-mail: quintanapablo@uniovi.es).

Francisco A. Juarez-Leon is with the Technological Institute of Celaya, Mexico.

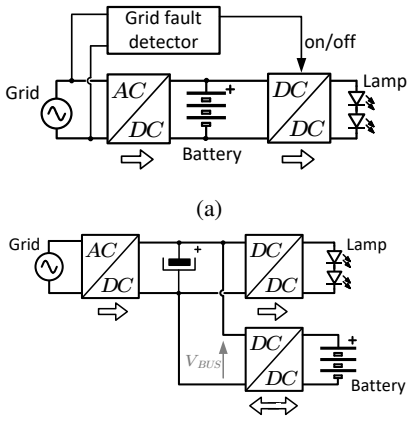

Fig. 1: Traditional block diagrams of emergency lighting systems: (a) Non-permanent. (b) Permanent.

and the production/manufacturing cost can be higher than other solutions (see Fig. 1b) [8]. Nevertheless, for very low power applications, the PFC stage can be replaced by a passive circuit, like a valley-fill.

2) Those involving two power converters: the one that charges the battery can drive the lamp during normal operation. If a fault occurs, then the lamp is supplied from the battery through a different power converter [10]. The efficiency of this proposal is usually lower than 90%, depending on the grid voltage.
3) Those involving integrated power converters: in [11] the authors combine two converters (the battery charger and the lamp driver) in one single magnetic core. This idea reduces the cost and size of the solution but also the overall efficiency of the system.

The aim of the present paper is to study and validate a new topology for a permanent emergency LED fixture with low component number and very high efficiency. This solution is based upon a series current regulator with two objectives: to drive the LED array and to charge the battery. This proposal avoids the use of two magnetic cores, one for the battery and one for the lamp, as in Fig. 1b. This series regulator needs to be very efficient to maximize the time interval on which the LED array can be on during a power outage. Hence, in order to achieve high efficiency it is important to reduce switching losses. One possible solution to this problem is to add resonant networks to standard DC-DC configurations [12], [13]. These techniques allow to operate at very high frequencies without severely compromising the efficiency due to the fact that the capacitor placed in parallel with the switch ensures a small dv/dt reducing the turn-off losses. Moreover, power loss during the turn-on is very small if ZVS condition is met.

In this work, the series regulator is based on a resonant converter whose input is placed in series with the LED lamp and the output resonant voltage is clamped by the battery, as shown in Fig. 2. This high frequency converter controls the LED current and the battery charging rate at the same time, making it a suitable solution for low power emergency

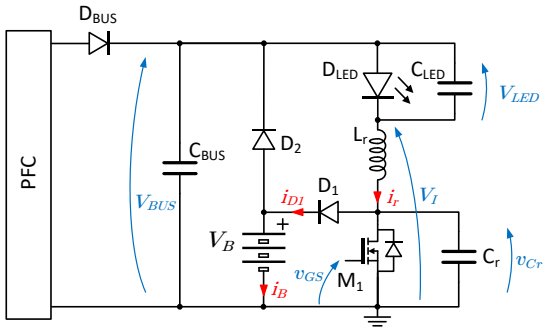

Fig. 2: Schematics of proposed circuit.

lamps. The current flowing through the lamp, and therefore, the battery, is controlled by means of the switching frequency. The higher the frequency, the lower the power handled by the converter and vice-versa. One of the main disadvantages of the proposed circuit is selecting the correct battery. As shown ahead, its voltage is directly related to the difference between the bus and the lamp voltages. Moreover, the PFC stage has to provide a low ripple, low voltage output (different solutions can be found in the literature [14]–[17]). This stage is out of the scope of the present work. Finally, although one power switch is required, this topology needs as well a small transistor in order to stop the charging process when the battery is fully charged. The proposed power converter derives from resonant Class-E inverters. Technically, this kind of converters can operate at switching frequencies over 1 MHz [18]–[22].

The rest of this paper is organized as follows. Section II presents a detailed description of the converter operation. In Section III, the equations are obtained using an energy balance approach. Section IV deals with the design procedure whereas practical results are reported in Section V. Finally, the conclusions of this work are presented.

II. Circuit Topology and Operation Principle

The basic waveforms of the proposed circuit during normal operation are depicted in Fig. 3. As can be seen, there are two resonant (dark gray) and two linear intervals (light gray). Within the resonant areas, the series converter behaves as an LC circuit.

When the transistor switches-off, the current begins to flow through the parallel resonant capacitor C_r, starting the first resonant stage (t_{cr}). The maximum voltage that this capacitor reaches is equal to the battery voltage due to the clamping diode D_1. While the capacitor voltage is clamped, the battery charges linearly during the t_{dr} interval. Once the current through the series resonant inductor, i_r, changes from positive to negative, the second resonant stage (t_{dr}) begins and therefore, the capacitor discharges over the inductor. The transistor must be switched on when the capacitor voltage reaches zero to ensure ZVS operation. From this point on, the inductor charges linearly (t_{on} interval) until its current reaches the maximum value, i_{rp}.

Diode D_2 is necessary whether there is a power cut or the battery is fully charged. It is worth pointing out that,

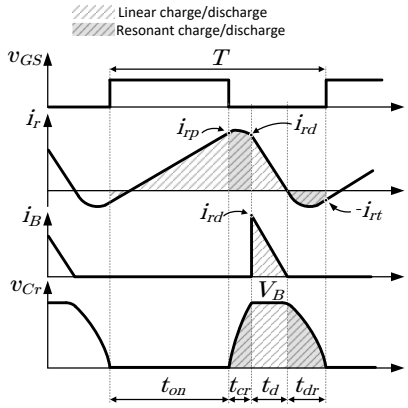

Fig. 3: Basic waveforms of the proposed resonant series regulator during normal operation (i.e. no power outage).

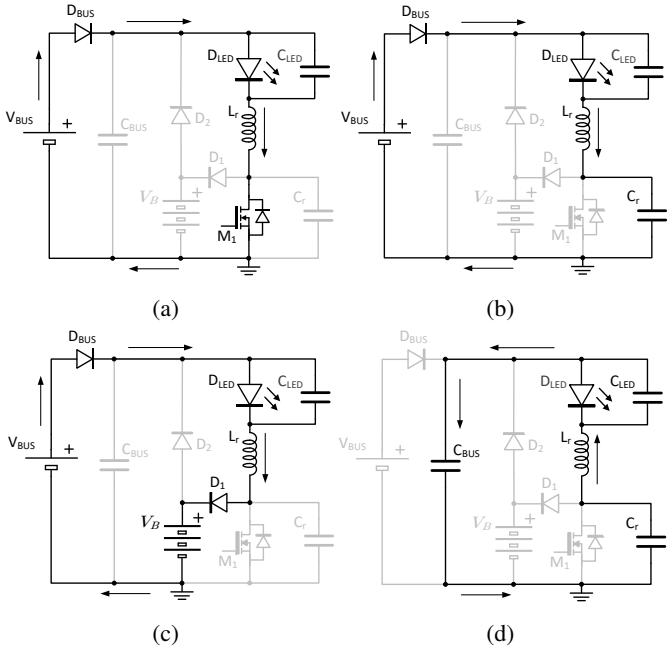

Fig. 4: Operation modes during normal operation: (a) t_{on} interval. (b) t_{cr} interval. (c) t_d interval. (d) t_{dr} interval.

under normal line supply, the converter functions as a regular electronic ballast and a charger, while under power failure, the converter will automatically switch to battery mode operation without any delay. Finally, diode D_{BUS} represents the classic output diode of the PFC. It also prevents energy from flowing backwards from the battery to the front-end power converter in the case of a grid fault.

Fig. 4 shows the different operation modes of the power converter assuming it is working under no power outage and the battery is not fully charged. If the battery was fully charged then diode D_2 would be directly biased during t_d interval. Nevertheless, during a power outage the battery supplies the lamp and diode D_{BUS} is reverse-biased. Unlike normal operation mode, the battery does not charge during any interval. In this case, during t_{on} and t_d intervals, diode D_2 is forward-biased.

III. Mathematical Analysis of the Converter

Rather complex methodologies that aim to model Class-E converters can be found in the literature [12], [23], [24]. However, in the present paper, the equations that describe the circuit behavior are obtained using energy balances during different operation intervals of the converter, which greatly simplify the mathematical analysis. In addition to that, two simplifications are done in order to carry out the analysis: first, parasitic components are not taken into consideration. Second, the difference between the bus voltage and the LEDs (V_I) is considered constant, meaning that the ripple of the bus voltage is neglected. Thus, the mathematical analysis is done in three steps:

1) Resonant charge of C_r (t_{cr}): The voltage waveform of capacitor C_r over one full switching is depicted in Fig. 3. However, one can firstly study the resonant charge of the capacitor that occurs during t_{cr}. The equivalent electric circuit during this interval is shown in Fig. 5a. Likewise, Fig. 6 shows the evolution of the voltage across the resonant capacitor in more detail. The ideal waveform is represented by a dotted gray line whereas the blue line is the actual voltage withstood by C_r. Notice that, ideally, the capacitor voltage would reach a peak value, V_{Crp}. As a matter of fact, that value is never reached because the capacitor is clamped by D_1 and the battery. This parameter will be useful later to obtain design equations and charts.

Assuming there is no power loss and that any voltage source in series with an LC circuit should be included in the energy balance as it was part of the initial charge of the capacitor, the energy balance between the inductor and the capacitor during t_{cr} interval is:

$$E_0 = E_1 \rightarrow \frac{1}{2}\cdot {i_{rp}}^2 \cdot L_r + \frac{1}{2}\cdot {V_I}^2 \cdot C_r = \frac{1}{2}\cdot {i_{rd}}^2 \cdot L_r + \\ + \frac{1}{2}\cdot (V_B - V_I)^2 \cdot C_r \quad (1)$$

where $V_I = V_{BUS} - V_{LED}$.

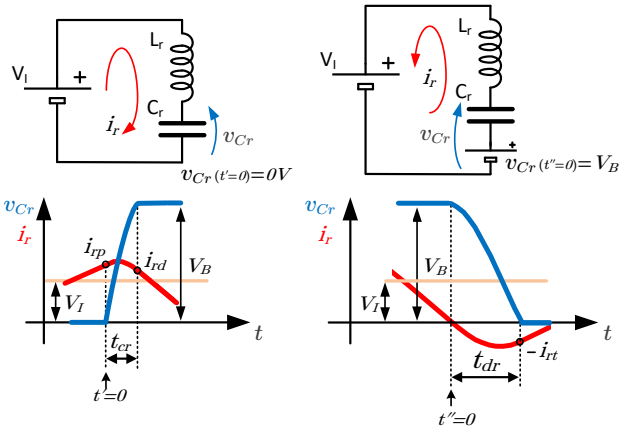

Fig. 5: Equivalent circuit during: (a) t_{cr} interval. (b) t_{dr} interval.

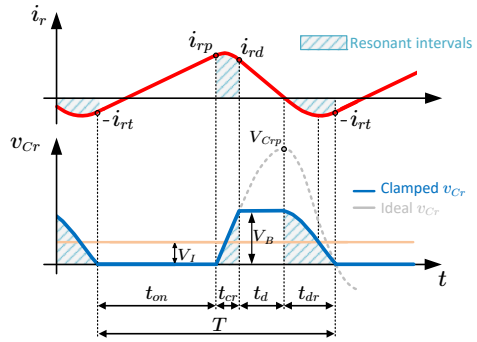

Fig. 6: Detailed evolution of i_r and v_{C_r}

Collecting terms:

$$\left({i_{rp}}^2 - {i_{rd}}^2\right) \cdot L_r = \left({V_B}^2 - 2 \cdot V_B \cdot V_I\right) \cdot C_r \tag{2}$$

The duration of this resonant charge is a fraction of a full resonant cycle. Therefore, it can be expressed as:

$$t_{cr} = \left[\arcsin\left(\frac{V_I}{V_{C_{rp}}}\right) + \arcsin\left(\frac{V_B - V_I}{V_{C_{rp}}}\right)\right] \cdot \sqrt{L_r \cdot C_r} \tag{3}$$

where $V_{C_{rp}}$ is the ideal peak value of the resonant voltage of the capacitor, as shown in Fig. 6. The expression of this variable can be obtained similarly to (1):

$$\frac{1}{2} \cdot {i_{rp}}^2 \cdot L_r + \frac{1}{2} \cdot {V_I}^2 \cdot C_r = \frac{1}{2} \cdot {V_{C_{rp}}}^2 \cdot C_r \Rightarrow$$
$$\Rightarrow V_{C_{rp}} = \sqrt{{i_{rp}}^2 \cdot \frac{L_r}{C_r} + {V_I}^2} \tag{4}$$

2) Resonant discharge of C_r (t_{dr}): At this point, another important relation can be obtained by analyzing the discharging interval of capacitor C_r. During t_{dr} interval, the capacitor discharges over the inductor like a classic resonant circuit. The equivalent electric circuit during this interval is shown in Fig. 5b. The main waveforms are illustrated again in Fig. 6 with more detail. During t_{dr}, the energy balance between the inductor and the capacitor can be studied and rearranged as:

$${i_{rt}}^2 = \left({V_B}^2 - 2 \cdot V_B \cdot V_I\right) \cdot \frac{C_r}{L_r} \tag{5}$$

From the previous equation, an important condition of the behavior of the circuit can be obtained:

$$V_B > 2 \cdot V_I \tag{6}$$

This limiting factor when designing this series regulator implies that if the difference between the bus and the lamp voltages increases, then the battery voltage also should. Thus, it is convenient that both bus and LED voltages are rather alike in order to work in a valid operation point. In the experimental setup used in this work, these voltages differ by 4.1 V.

Similar to (3) and from Fig. 6, the duration of the resonant discharge can be defined as a fraction of a full resonant sine wave:

$$t_{dr} = \left[\frac{\pi}{2} + \arcsin\left(\frac{V_I}{V_B - V_I}\right)\right] \cdot \sqrt{L_r \cdot C_r} \tag{7}$$

3) Linear charge and discharge of L_r (t_{on} / t_d): The energy balance in the reactive components during t_{cr} and t_{dr} intervals is equal to zero. One can assume that if C_{LED} is big enough to keep the lamp voltage stable, it does not interfere with the resonance between L_r and C_r. Therefore, the whole LED array plus the capacitor set behaves as an ideal voltage source. This behavior is based upon the fact that the impedance of the capacitor at high frequencies is small enough to carry all the high frequency components of the current, whereas the DC component flows through the LEDs. However the parasitic elements of the lighting semiconductors can lead to small discrepancies with the theoretical calculations. In any case, the error between these last two is negligible.

Based on these assumptions, the expression of the average LED current can be written as:

$$\bar{i}_{LED} = \left(\frac{i_{rp} - i_{rt}}{2}\right) \cdot \frac{t_{on}}{T} + \frac{i_{rd}}{2} \cdot \frac{t_d}{T} \tag{8}$$

Both linear intervals t_d and t_{on} can be studied as in classic power converters, yielding the following expressions:

$$t_d = \frac{i_{rd} \cdot L_r}{(V_B - V_I)} \tag{9}$$

$$t_{on} = \frac{(i_{rp} + i_{rt}) \cdot L_r}{V_I} \tag{10}$$

From Fig. 3, the average value of the battery current can be defined as:

$$\bar{i}_B = \frac{i_{rd}}{2} \cdot \frac{t_d}{T} \tag{11}$$

Combining (9) and (11), the final expression of the average current through the battery is obtained:

$$\bar{i}_B = \frac{{i_{rd}}^2 \cdot L_r}{2 \cdot T \cdot (V_B - V_I)} \tag{12}$$

An equation that will be useful later to define the design charts and relates three important current values in Fig. 3 can be acquire by merging (2) and (5):

$${i_{rt}}^2 = {i_{rp}}^2 - {i_{rd}}^2 \tag{13}$$

Equation (8) depends on many variables and it is difficult to handle when designing the converter. Hence, it is advisable to get it simplified by combining it with (9), (10) and (13):

$$\bar{i}_{LED} = \frac{{i_{rd}}^2 \cdot L_r}{2 \cdot T \cdot V_I} + \frac{{i_{rd}}^2 \cdot L_r}{2 \cdot T \cdot (V_B - V_I)} \tag{14}$$

The last step of the analysis of the currents can be done by dividing (12) over (14). The relation between the LED and battery average currents can be represented as a function of the voltages V_{BUS}, V_{LED}, and V_B:

$$\frac{\bar{i}_B}{\bar{i}_{LED}} = \frac{\frac{1}{V_B - V_I}}{\frac{1}{V_I} + \frac{1}{V_B - V_I}} = \frac{V_I}{V_B} \tag{15}$$

This last expression denotes that all those signals are not decoupled. As the battery voltage rises, the battery current is reduced, keeping constant the ratio $\frac{\bar{i}_B}{\bar{i}_{LED}}$. In order to prevent the battery from overcharging, it has to be disconnected by

hardware when the maximum voltage is reached. This issue will be addressed in Section V.

Finally, the expression of the switching period T is the combination of (3), (4), (7), (9), and (10):

$$\begin{aligned} T = t_{on} + t_d + t_{cr} + t_{dr} = \\ = \frac{(i_{rp} + i_{rt}) \cdot L_r}{V_I} + \frac{i_{rd} \cdot L_r}{V_B - V_I} + \\ + \left[\arcsin\left(\frac{V_I}{\sqrt{{i_{rp}}^2 \cdot \frac{L_r}{C_r} + {V_I}^2}} \right) + \right. \\ + \arcsin\left(\frac{V_B - V_I}{\sqrt{{i_{rp}}^2 \cdot \frac{L_r}{C_r} + {V_I}^2}} \right) + \\ \left. + \frac{\pi}{2} + \arcsin\left(\frac{V_I}{V_B - V_I} \right) \right] \cdot \sqrt{L_r \cdot C_r} \end{aligned} \quad (16)$$

IV. Design Procedure

In the proposed topology, there are two components that must be calculated to complete the design: capacitor C_r and inductor L_r. The design methodology followed by the authors in order to obtain these values is explained ahead. One can begin by choosing the lamp and then the battery and the nominal bus voltage. In this section, the design curves of the proposed converter are shown.

Regarding this application, Li-ion batteries are usually a good choice. They have high energy density, low self-discharge, low maintenance, and the charging methods are well known [25]–[28]. As stated in (15), the battery charging rate is related to V_I. Thus, V_{BUS} cannot be too small. In order to comply with both (6) and (15), a valid solution is to use three 18650 Li-ion batteries placed in series ($V_{B_{nom}}$= 10.6 V) and a nominal bus voltage of 12.6 V. Design specifications of the converter are given in Table I.

Once the specifications have been defined, the first step of the design procedure is to calculate the resonant capacitor, C_r. This calculation is better tackled by means of a chart. From (15), the average current coming to the battery under normal operation (no grid failure and nominal battery voltage) is calculated. Then, a parameter q can be defined as the product ${i_{rd}}^2 \cdot L_r$. Combined with (12), one can obtain:

$$q = \bar{i}_B \cdot 2 \cdot T \cdot (V_B - V_I) \quad (17)$$

where it is noticeable that parameter q strongly depends upon the switching frequency.

TABLE I: Design specifications

Bus voltage V_{bus}= 12.6 V	Nominal battery voltage $V_{B_{nom}}$= 10.6 V	Nominal frequency 220 kHz
Lamp current/voltage 0.5 A / 8.5 V	LED max. values 180 mA / 3.1 V	LED model NFSW757H-V1

A second design parameter m can be defined as the ratio between the currents i_{rp} and i_{rt}:

$$m = \frac{i_{rp}}{i_{rt}} \quad (18)$$

From (5), (17), and (18), the expression of the resonant capacitor is achieved:

$$C_r = \frac{q}{(m^2 - 1) \cdot \left({V_B}^2 - 2 \cdot V_B \cdot V_I \right)} \quad (19)$$

The numerical solution of this expression is shown in Fig. 7. On one hand, small values of m imply bigger capacitances (Fig. 7c) so for these design conditions, it is recommendable to operate between 4 and 6. On the other hand, high q values yield low switching frequencies (Fig. 7b). This kind of resonant converters are able to work at very high frequencies without losing efficiency. Hence, in this example, trade-off values of $1.15 \cdot 10^{-5}$ and 5 were set for the parameters q and m, respectively. From Fig. 7, the required resonant capacitor is thus around 17 nF.

In order to address the calculation of the resonant inductor, one can observe that it has influence over many parameters on the circuit, i.e., the switching frequency, as seen in (16). Moreover, the duration of t_{cr} is also determined by a third party parameter: $V_{C_{rp}}$. Therefore, it is advisable to obtain the numerical solution of (4) and (16) as a function of the resonant inductor and the current i_{rp}. As depicted in Fig. 8, big values of the inductor or the current imply high $V_{C_{rp}}$ voltages. A similar condition is applied to i_{rp}. Big peak currents involve a high $V_{C_{rp}}$ and hence, a succinct resonant stage. A similar scenario is shown in Fig. 9, where small values of L_r and i_{rp} imply very high switching frequencies. Consequently, the decision over L_r and i_{rp} is not arbitrary; it must comply with a reasonable switching frequency as well as with the desired average LED current. In the present work, authors have decided to choose an inductor of 6 μH and an i_{rp} of around 1.4 A yielding a nominal switching frequency of 220 kHz. This process is iterative and the solution is not unique.

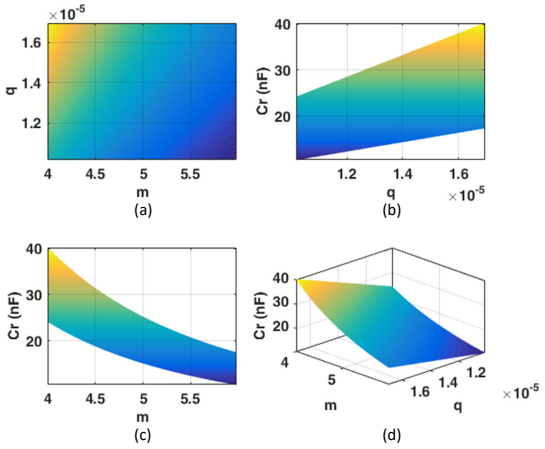

Fig. 7: Calculation of C_r capacitor.

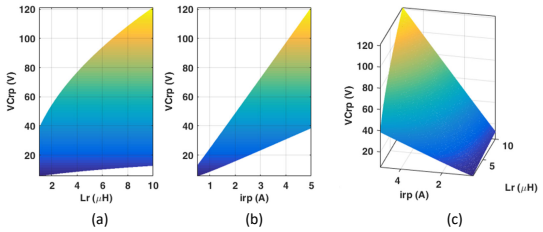

Fig. 8: Calculation of $V_{C_{rp}}$.

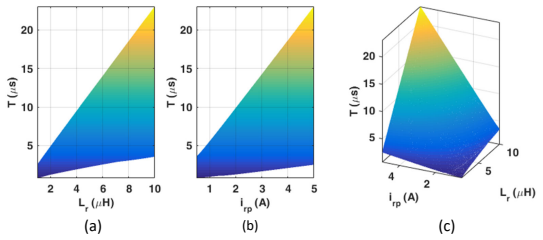

Fig. 9: Calculation of the switching period.

V. Experimental Results

A prototype with regular and emergency lighting features has been designed and implemented to verify the feasibility of the proposed power converter. A compromise solution based upon all previous design charts is shown in Table II.

TABLE II: Calculated and measured parameters of the converter

Symbol	Theoretical value	Simulated value	Measured value
L_r	6 μH	6 μH	6.04 μH - ESR = 33 mΩ @ 220 kHz
C_r	17 nF	17 nF	16.8 nF
C_{LED}	1.2 μF	1.2 μF	1.15 μF
C_{BUS}	3440 nF	3440 nF	3416 nF (3 μF ceramic, 440 nF MKP)
t_{on}	2.49 μs	2.63 μs	2.49 μs
t_d	1.25 μs	956 ns	0.89 μs
t_{cr}	120.41 ns	160 ns	98 ns
t_{dr}	711.97 ns	749 ns	702 ns

Semiconductors

Symbol	Reference	Electrical characteristics
M_1	IRF530	$R_{DS_{(on)}} = 0.16\ \Omega$, $C_{oss} = 250\ pF$
D_1, D_2	11DQ10	$V_F = 0.5\ V$ @ $T_J = 125\ ^oC$

A. Control strategy

One of the main objectives of this manuscript is to test the feasibility of a novel series resonant converter for a permanent emergency lamp. However, the control strategy represents an important part to obtain the desired behavior. That way, a frequency control scheme is used to regulate the current through the LED lamp. This current can be either measured directly with a current sensor with high common-mode rejection ratio (CMRR) or indirectly by means of a couple resistors in the return path to the power source (DC bus or battery). Notice that switching frequency and power are inversely proportional in this power electronic converter, meaning that the higher the frequency, the lower the current.

Regarding the battery charging process, several techniques can be found in the bibliography, such as constant-trickle-current charging, constant-current charging (CC), and constant-current constant-voltage charging (CC-CV) [25], [26]. Due to the proposed design methodology, the current flowing through the battery slowly decreases until it reaches almost zero. The behavior is therefore, similar to a CC-CV algorithm. However, this current never reaches zero amperes and at some point, the charging needs to be stopped by hardware in order to not overcharge the electrochemical device. A small transistor (battery protection unit, or BPU) in series with the battery operating as a protection device is thus required. This semiconductor does not switch at high frequencies. It opens and closes the battery circuit as a protection . Hence, a small low-cost bipolar transistor working in the cut-off and saturation regions is enough. The efficiency of the overall system is slightly affected if the collector-emitter saturation voltage is small (see Fig. 10).

In this manuscript, a digital control based on a microcontroller is proposed to control the state of the battery as well as the current flowing through the LEDs. A low pin count, medium-density performance device like a STM32F103CBT6 can properly perform. The battery charging process is slow, meaning that the calculation of the current reference is not a critical task that affects the dynamics of the converter. The peak current i_{rp} is the control variable of the system since it points out the end of the lineal interval t_{on}. Although i_{rd} is the control current in (14), a change of variable can be easily performed by means of (13) and (18). The PI controller establishes the switching frequency depending on the error but an additional synchronization block is required in order to maintain ZVS operation, detecting when the resonant capacitor is fully discharged. An equivalent block diagram of the feedback control scheme is shown in Fig. 10.

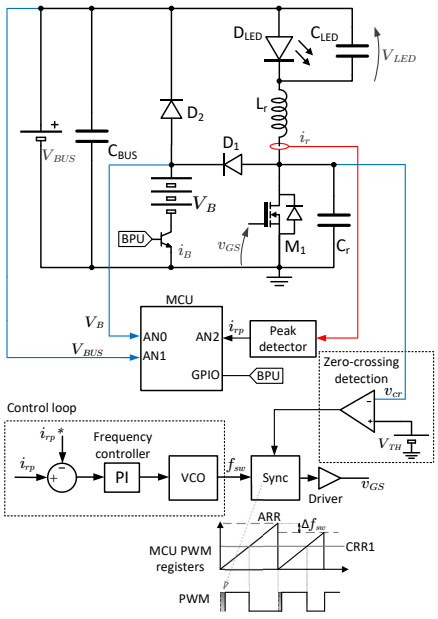

Fig. 10: Control strategy.

B. Experimental results

A laboratory prototype has been built to test the feasibility of the proposal, as shown in Fig. 11. Figs. 14a to 14d show the behavior of the power converter in steady-state with a constant input voltage. The experimental results of the circuit operating in normal mode, i.e., during no power fault are depicted in Fig. 14a. Resonant and LED currents as well as the PWM control signal and the capacitor voltage waveforms are illustrated. In this experiment, the battery is charged at its nominal voltage of 10.6 V. The current flowing through the battery under the same conditions as before is shown in Fig. 14b. The ZVS operation is kept all the time and the waveforms are quite similar to the theoretical ones represented in Fig. 3.

Fig. 14c shows the effect of having the battery almost charged. Part of the current is sent back to the DC bus through recirculation diode D_2 (CH2) while the remaining goes to the battery (CH1). The current through the LEDs is kept constant while CC-CV control is naturally achieved, preventing the battery from getting damaged.

The waveforms of currents and voltages during fault operation are shown in Fig. 14d. The operation frequency and peak current values are reduced in order to keep the nominal current through the lamp.

The response of the power converter to disturbances in the input voltage is shown in Figs. 14e and 14f. Both figures include zoomed areas of the waveforms. The dynamics of this power converter are extremely fast, making it simple to compensate for 100-120 Hz perturbations in the bus voltage using the proposed PI controller (provided that the converter operates inside the linear region and ZVS condition is met). The AC impedance of the LED lamp combined with capacitor C_{LED} is negligible at 100-120 Hz, and both the resonant inductor and capacitor are really small, meaning that the converter reacts almost instantaneously compared to the expected perturbations. The dynamics are, therefore, not critical for the application. Fig. 14e shows the effect of a 100 Hz perturbation in the input bus voltage with the converter operating in open-loop. As it can be seen, there is no delay between the perturbation signal and the filtered LED current. Fig. 14e shows the same traces with the control enabled. The LED current ripple is noticeably reduced.

Finally, the basic goal of permanent emergency lighting systems is to provide sufficient lighting during power outages thus dimming is not a feature that is normally implemented. However, this topology allows to reduce the current though the LEDs to an extent. In order to show the dimming capability of the converter, the basic waveforms of the power converter at 50% are shown in Fig. 12. It can be noticed that the frequency increases while the peak resonant current is slightly reduced. Dimming below 30% is not recommendable in this power converter due to changes in the operation intervals. The resonant capacitor does not clamp during the resonant interval and therefore, battery is never charged.

The efficiency of the power converter as a function of the lamp current is depicted in Fig. 13. This chart shows the efficiency when the power converter operates under no fault condition and during a power cut (fully charged battery).

VI. Conclusion

In this manuscript, a permanent emergency lamp based on a series current resonant regulator has been presented. This topology has been placed in series with the LED, operating as a controllable non-dissipative impedance, yielding minimal switching losses. Besides, the emergency lamp battery is charged by means of a clamping diode, thus avoiding this way the need of a different power converter. This means that a single power converter is able to control the current through the lamp and charge the emergency battery at the same time, providing a seamless transition between normal and grid fault operation modes.

The circuit behavior during all the operation intervals has been analyzed. This analysis has been oriented to obtain a set of charts that allow a straightforward design and calculation of all the circuit components. Based on the proposed procedure, a design laboratory prototype has been built and tested.

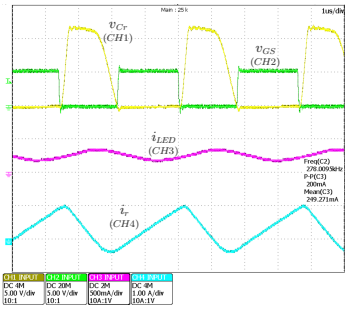

Fig. 12: Basic circuit waveforms at nominal battery voltage and 50% dimming.

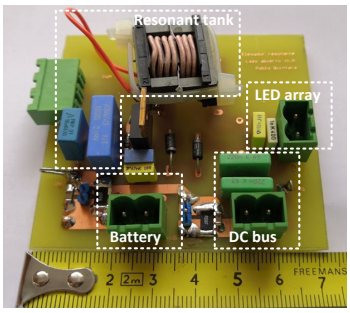

Fig. 11: Prototype of the proposed power converter.

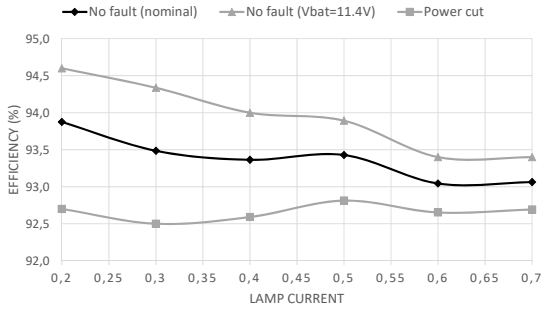

Fig. 13: Measured efficiency as a function of the LED current.

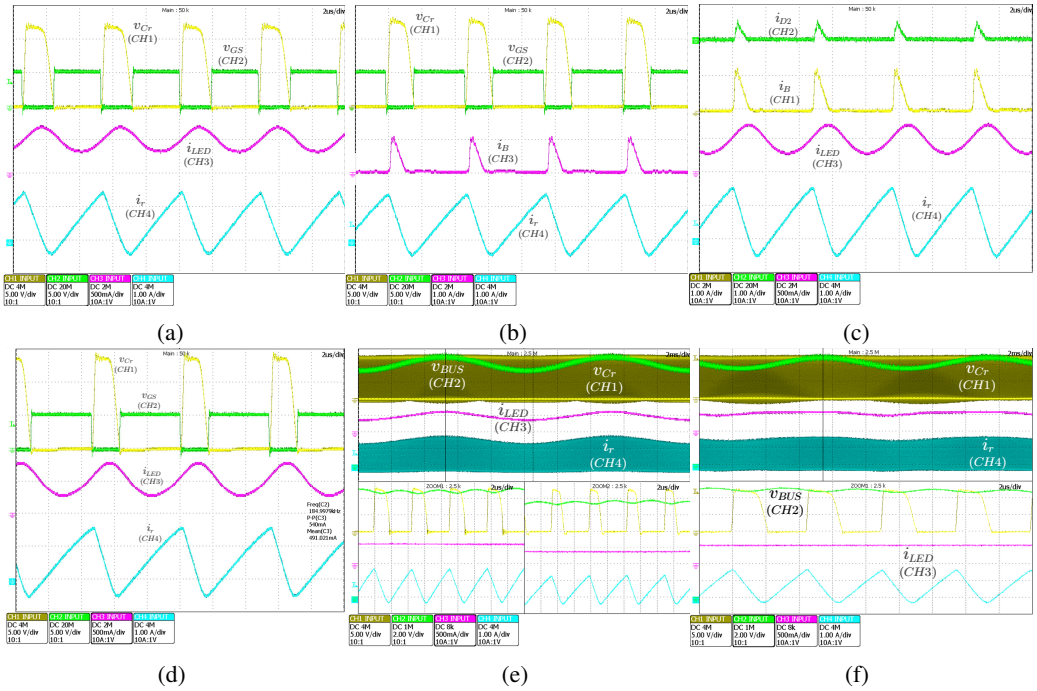

Fig. 14: Experimental results: (a) Basic circuit waveforms at nominal battery voltage. (b) Current flowing to the battery during charging time. (c) Currents through LEDs, battery and diode D_2 when state of charge of the battery is at 90%. (d) Basic circuit waveforms during fault operation and battery fully charged. (e) Open-loop operation. (f) Closed-loop operation.

Several laboratory tests have been performed on the prototype in order to evaluate the feasibility of the proposal. First, during normal operation mode, the power converter controlled the current flowing through the lamp and the battery, maintaining ZVS and high efficiency. During a power outage, the battery supplied the lamp and, therefore, waveforms changed (in terms of frequency and peak values). Nevertheless, good efficiency as well as ZVS condition were kept.

ACKNOWLEDGMENT

This work has been supported by the Ministry of Science and Innovation of the Government of Spain under Research Grant PID2019-105568RB-I00.

REFERENCES

[1] *IEC 60598-2-22:2014+AMD1:2017. Luminaires - Part 2-22: Particular requirements - Luminaires for emergency lighting*, International Electrotechnical Commision Std., Sep. 2017.

[2] *IEC 61347-1:2015+AMD1:2017. Lamp controlgear - Part 1: General and safety requirements*, International Electrotechnical Commision Std., Sep. 2017.

[3] *IEC 60364-1:2005. Low-voltage electrical installations*, International Electrotechnical Commision Std., Nov. 2005.

[4] *ISO 30061:2007.Emergency lighting*, International Organization for Standardization Std., Nov. 2007.

[5] Y. Wu and Y. Chen, "A three-in-one converter for regular and emergency lighting applications," *IEEE Transactions on Industry Applications*, vol. 45, DOI 10.1109/TIA.2008.2009907, no. 1, pp. 108–115, 2009.

[6] *IEC 62386: International Standard for the Digital Addressable Lighting Interface*, International Organization for Standardization Std., Apr. 2020.

[7] J. M. Alonso, P. J. Villegas, J. Diaz, C. Blanco, and M. Rico, "A microcontroller-based emergency ballast for fluorescent lamps," *IEEE Transactions on Industrial Electronics*, vol. 44, DOI 10.1109/41.564159, no. 2, pp. 207–216, 1997.

[8] M. Rico-Secades, A. J. Calleja, J. Ribas, E. L. Corominas, J. M. Alonso, J. Cardesin, and J. Garcia-Garcia, "Evaluation of a low-cost permanent emergency lighting system based on high-efficiency leds," *IEEE Transactions on Industry Applications*, vol. 41, DOI 10.1109/TIA.2005.853389, no. 5, pp. 1386–1390, 2005.

[9] R. A. Pinto, M. R. Cosetin, M. Cervi, A. Campos, and R. N. do Prado, "Emergency lamp using high-brightness led," in *2011 IEEE International Symposium on Industrial Electronics*, DOI 10.1109/ISIE.2011.5984167, pp. 257–262, 2011.

[10] R. A. Pinto, M. R. Cosetin, A. Campos, M. A. Dalla Costa, and R. N. do Prado, "Compact emergency lamp using power leds," *IEEE Transactions on Industrial Electronics*, vol. 59, DOI 10.1109/TIE.2011.2159352, no. 4, pp. 1728–1738, 2012.

[11] J. Cardesin, J. Ribas, J. Garcia-Garcia, M. Rico-Secades, A. Javier Calleja, E. Lopez Corominas, and M. A. Dalla Costa, "Led permanent emergency lighting system based on a single magnetic component," *IEEE Transactions on Power Electronics*, vol. 24, DOI 10.1109/TPEL.2009.2013138, no. 5, pp. 1409–1416, 2009.

[12] J. Ribas, P. J. Quintana-Barcia, J. Cardesin, A. J. Calleja, and E. L. Corominas, "Led series current regulator based on a modified class-e resonant inverter," *IEEE Transactions on Industrial Electronics*, vol. 65, DOI 10.1109/TIE.2018.2822618, no. 12, pp. 9488–9497, 2018.

[13] J. Ribas, P. J. Quintana, J. Cardesin, A. J. Calleja, and J. M. Lopera, "Closed loop control of a series class-e voltage-clamped resonant converter for led supply with dimming capability," *Electronics*, vol. 8, DOI 10.3390/electronics8121380, no. 12, 2019. [Online]. Available: https://www.mdpi.com/2079-9292/8/12/1380

[14] onsemi, *ON Semiconductor Application Notes AND8318/D*, Sep. 2008. [Online]. Available: https://www.onsemi.com/pub/Collateral/AND8318-D.PDF

[15] onsemi, *ON Semiconductor Application Notes AND8460/D*, Aug. 2010. [Online]. Available: https://www.onsemi.com/pub/collateral/and8460-d.pdf

[16] O. Garcia, J. Cobos, P. Alou, R. Prieto, and J. Uceda, "A high efficient low output voltage (3.3 v) single stage ac/dc power factor correction converter," in *APEC '98 Thirteenth Annual Applied Power Electronics Conference and Exposition*, vol. 1, DOI 10.1109/APEC.1998.647692, pp. 201–207 vol.1, 1998.

[17] P. S. Almeida, D. Camponogara, M. Dalla Costa, H. Braga, and J. M. Alonso, "Matching led and driver life spans: A review of

different techniques," *IEEE Industrial Electronics Magazine*, vol. 9, DOI 10.1109/MIE.2014.2352861, no. 2, pp. 36–47, 2015.
[18] H. Yogi, X. Wei, H. Sekiya, and T. Hikihara, "Design of 6.78 mhz sic mosfet class-e inverter with a class-Î¦ high-speed driver," in *2019 IEEE Energy Conversion Congress and Exposition (ECCE)*, DOI 10.1109/ECCE.2019.8912609, pp. 375–379, 2019.
[19] H. Hase, H. Sekiya, J. Lu, and T. Yahagi, "Resonant dc-dc converter with class-e oscillator," *IEEE Transactions on Circuits and Systems I: Regular Papers*, vol. 53, DOI 10.1109/TCSI.2006.880341, no. 9, pp. 2025–2035, 2006.
[20] C. Li and Y. Yam, "Maximum frequency and optimum performance of class e power amplifiers," 1994.
[21] S. Dehghani and T. Johnson, "A 2.4-ghz cmos class-e synchronous rectifier," *IEEE Transactions on Microwave Theory and Techniques*, vol. 64, DOI 10.1109/TMTT.2016.2547393, no. 5, pp. 1655–1666, 2016.
[22] K. Datta and H. Hashemi, "Performance limits, design and implementation of mm-wave sige hbt class-e and stacked class-e power amplifiers," *IEEE Journal of Solid-State Circuits*, vol. 49, DOI 10.1109/JSSC.2014.2353800, no. 10, pp. 2150–2171, 2014.
[23] C. Bernal, E. Oyarbide, P. Molina Gaudo, and A. Mediano, "Dynamic model of class-e inverter with multifrequency averaged analysis," *IEEE Transactions on Industrial Electronics*, vol. 59, DOI 10.1109/TIE.2012.2185012, no. 10, pp. 3737–3744, 2012.
[24] N. Bertoni, G. Frattini, R. G. Massolini, F. Pareschi, R. Rovatti, and G. Setti, "An analytical approach for the design of class-e resonant dc-dc converters," *IEEE Transactions on Power Electronics*, vol. 31, DOI 10.1109/TPEL.2016.2535387, no. 11, pp. 7701–7713, 2016.
[25] M. M. Alhaider, E. M. Ahmed, M. Aly, H. A. Serhan, E. A. Mohamed, and Z. M. Ali, "New temperature-compensated multi-step constant-current charging method for reliable operation of battery energy storage systems," *IEEE Access*, vol. 8, DOI 10.1109/ACCESS.2020.2972391, pp. 27 961–27 972, 2020.
[26] D. Ansean, V. M. Garcia, M. Gonzalez, C. Blanco-Viejo, J. C. Viera, Y. F. Pulido, and L. Sanchez, "Lithium-ion battery degradation indicators via incremental capacity analysis," *IEEE Transactions on Industry Applications*, vol. 55, DOI 10.1109/TIA.2019.2891213, no. 3, pp. 2992–3002, 2019.
[27] L. Chen, S. Wu, D. Shieh, and T. Chen, "Sinusoidal-ripple-current charging strategy and optimal charging frequency study for li-ion batteries," *IEEE Transactions on Industrial Electronics*, vol. 60, DOI 10.1109/TIE.2012.2186106, no. 1, pp. 88–97, 2013.
[28] Y. Li, K. Li, Y. Xie, J. Liu, C. Fu, and B. Liu, "Optimized charging of lithium-ion battery for electric vehicles: Adaptive multistage constant-current constant voltage charging strategy," *Renewable Energy*, vol. 146, DOI https://doi.org/10.1016/j.renene.2019.08.077, pp. 2688–2699, 2020.

Pablo Quintana-Barcia (S'13-M'16) was born in Tapia de Casariego, Spain, in 1987. He received the M.Sc. in electrical engineering and the Ph.D. degree in power electronics both from the University of Oviedo, Spain in 2011 and 2015 respectively. In September 2011, he joined the Electrical and Electronic Engineering Department at the University of Oviedo, where he is currently an Assistant Professor. He is a member of the Efficient Energy Conversion, Industrial Electronics and Lighting research group (CE3I2) of the University of Oviedo. Dr. Quintana's research interests include power electronics and control for industrial, grid support, and lighting applications.

Javier Ribas (S'97-M'04-SM'12) was born in Milwaukee, U.S., in 1971. He received the M.Sc. and PhD degrees in Industrial Engineering both from the University of Oviedo, Spain, in 1995 and 2001 respectively. Since 1996 he has been working within the Department of Electrical Energy of the University of Oviedo where he is currently an Associate Professor. He is an active member of the CE3I2 research group of the University of Oviedo. His research interests include electronic lighting systems, solid state lighting, switched-mode power supplies and high-power-factor rectifiers. Dr. Ribas is co-author of more than twenty journal papers and more than seventy international conference papers in industrial and power electronics.

Francisco A. Juarez-Leon (S'20) was born in Guanajuato, Mexico, in 1993. He received the B.S. degree in electronics engineering and the M.Sc. in power electronics from the Technological Institute of Celaya, Mexico, in 2017 and 2021 respectively. He is currently carrying out his Ph.D. in McMaster University, Canada. His research interests include power conversion, mathematical modeling of power converters, control theory applied to power electronics, and advanced digital systems.

Diego Rodriguez-Fuentes Diego Rodriguez Fuertes was born in Oviedo, Spain, in 1997. He received the M.Sc. degree in Automation Engineering from the University of Oviedo, Spain, in 2021. In 2019, he joined the CE3I2 research group of the University of Oviedo where he is currently developing his Ph.D studies. His research interests include power conversion for lighting and electronic vehicles.